Biogeochemical feedbacks to ocean acidification in a cohesive photosynthetic sediment

Kay Vopel[1*], Alexis Marshall[2], Shelly Brandt[2], Adam Hartland[3], Charles K. Lee[3], S. Craig Cary[2], Conrad A. Pilditch[2]

[1]School of Science, Auckland University of Technology, Private Bag 92006, Auckland, New Zealand

[2]School of Science, University of Waikato, Private Bag 3105, Hamilton, New Zealand

[3]Environmental Research Institute, School of Science, University of Waikato, Private Bag 3105, Hamilton, New Zealand

*corresponding author, kay.vopel@aut.ac.nz, phone: +64212214242

Ecosystem feedbacks in response to ocean acidification can amplify or diminish the diel pH oscillations that characterize productive coastal waters. We report that benthic microalgae generate such oscillations in the porewater of cohesive sediment and ask how carbonation (acidification) of the overlying seawater alters these in the absence and presence of biogenic calcite. To do so, we placed a 1-mm layer of ground oyster shells (Treatment) or sand (Control) onto intact sediment cores free of large dwelling fauna, and then gradually increased the pCO_2 in the seawater above half of the Treatment and Control cores from 472 to 1216 µatm (pH 8.0 to 7.6, CO_2:HCO_3^- from 4.8 to 9.6 x 10^{-4}). Vertical porewater [O_2] and [H^+] microprofiles measured 16 d later showed that this carbonation had decreased O_2 penetration in all cores, indicating a metabolic response. In carbonated seawater: (1) sediment biogeochemical processes added and removed more H^+ to and from the porewater in darkness and light, respectively, than in ambient seawater *increasing* the amplitude of the dark–light porewater [H^+] oscillations, and (2) the dissolution of calcite decreased the porewater [H^+] below that in overlying seawater, reversing the dark sediment–seawater H^+ flux and *decreasing* the amplitude of diel [H^+] oscillations. This dissolution did not, however, counter the negative effect of carbonation on sediment O_2 penetration. We hypothesise that the latter effect and the observed enhanced acidification of the sediment porewater were caused by an ecosystem feedback: a CO_2-induced increase in the microbial reoxidation of reduced solutes with O_2.

Introduction

Dissolution of anthropogenic CO_2 in the ocean alters the speciation of dissolved inorganic carbon (DIC), increasing seawater $[H^+]$ while decreasing its carbonate saturation state (Ω) and buffering capacity—the latter property being described by the Revelle factor (Revelle and Suess 1957, Frankignoulle 1994, Egleston et al. 2010). A reduction in this buffering capacity implies that repeated *addition* of a fixed quantity of CO_2 results in progressively larger increases in $[H^+]$. Repeated *removal* of a fixed quantity of CO_2 decreasing seawater $[H^+]$ and increasing buffering capacity results in progressively smaller decreases in $[H^+]$. In other words, the future ocean will be more sensitive to CO_2 dynamics than is presently the case and we expect the current trends of increasing average seawater $[H^+]$ (Bates et al., 2014; Lauvset et al., 2015; Ríos et al., 2015) to be accompanied by an increase in the peak-to-peak amplitude of diel and seasonal variations in seawater $[H^+]$ (see, e.g., Schulz and Riebesell 2012). If we now consider the possibility that biota conditioned to current diel and seasonal variations may respond to changes in the magnitude of these variations, independent of changes in the mean seawater carbonate chemistry, then knowledge of the effects of ocean acidification on these variations becomes important.

In productive coastal environments, metabolic (e.g., photosynthesis and respiration) and geochemical (e.g., precipitation and dissolution) processes cause diel and seasonal variations in the local seawater chemistry that are similar or larger than the variation in ocean chemistry predicted for the 21st century (Provoost et al. 2010, Hoffman et al. 2011)—their magnitude being a function of the local solute transport regime (Jury et al. 2013). Feedback from these processes in response to ocean acidification can enhance or diminish trends in both the mean seawater carbonate chemistry and the diel and seasonal chemistry variations, but this depends on the mechanisms involved and their intensity. Some evidence for this exists for ecosystems in which solute exchange with the open ocean is limited (Borges and Gypens 2010, Jury et al. 2013, Hagens et al. 2015).

Eutrophication is one example where local conditions can amplify the positive effect of ocean acidification on variations in seawater $[H^+]$ by increasing primary production, which in turn tends to increase respiration (Borges and Gypens 2010, Cai et al. 2011, Sunda and Cai 2012). Modelling diel seawater chemistry variations in a coastal, reef flat ecosystem, Jury et al. (2013) reported that the extent to which an increase in offshore pCO_2 (ocean acidification, to

900 µatm) and warming (+3 °C) increased these variations depended on the kind and intensity of ecosystem feedback mechanisms involved and the seawater residence time. As seawater residence time and feedback intensity increased, daytime seawater chemistry became more similar to present-day conditions while night-time seawater chemistry became less similar to present-day conditions. In this case, feedbacks increased the diel $[H^+]$ variations by a factor of up to 2.5. In other systems, limitations in vertical solute exchange serve to enhance ecosystem feedbacks: Hagens et al. (2015), for example, found differences in the magnitude of seasonal $[H^+]$ fluctuations between the surface and bottom layer of a seasonally stratified coastal lake and attributed these differences to a substantial reduction in the acid–base buffering capacity of the hypoxic (CO_2 enriched) bottom water in the summer period.

Here, we examine this concept to the seawater boundary of cohesive photosynthetic sediment, which hosts a network of microbial reaction processes that operates at much smaller spatial scales. Solute transport in the millimetre-thick reactive layer that separates the free-flowing seawater from the deeper anoxic sediment is limited by molecular diffusion and therefore, the microbial processes in this layer create steep, measurable gradients and strong diel oscillations in porewater $[H^+]$ and $[O_2]$. We argue that feedbacks in response to ocean acidification occurring at this interface matter for ecosystem-scale processes. This is because the environmental conditions at the sediment–water interface in the coastal ocean affect important processes including the remineralisation of organic carbon, nitrogen cycling, reactive solute exchange between the sediment and the overlying seawater, larval settlement, recruitment, faunal emergence and the behaviour of key bioturbating species (e.g., Santschi et al. 1990, Pawlik 1992, Marinelli and Woodin 2002, Clemens and Hunt 2015).

Previously we found that experimental carbonation (acidification) of seawater overlying subtidal silt sediment shifted porewater $[H^+]$ profiles measured in light and darkness towards higher concentrations and that this shift extended to the depth of the anoxic sediment (Vopel et al. 2021). We now ask how such carbonation alters the diel oscillations in porewater $[H^+]$ and $[O_2]$ and if the dissolution of biogenic calcite can dampen the amplitude of these oscillations. Besides porewater buffering, carbonation-induced dissolution of calcite at the sediment surface may also have implications for recruitment of calcifying fauna (e.g., Clements et al. 2016). In our design, we included measurements of porewater $[O_2]$ as a proxy

of microbial metabolic activity to assess possible metabolic feedbacks to experimental seawater carbonation.

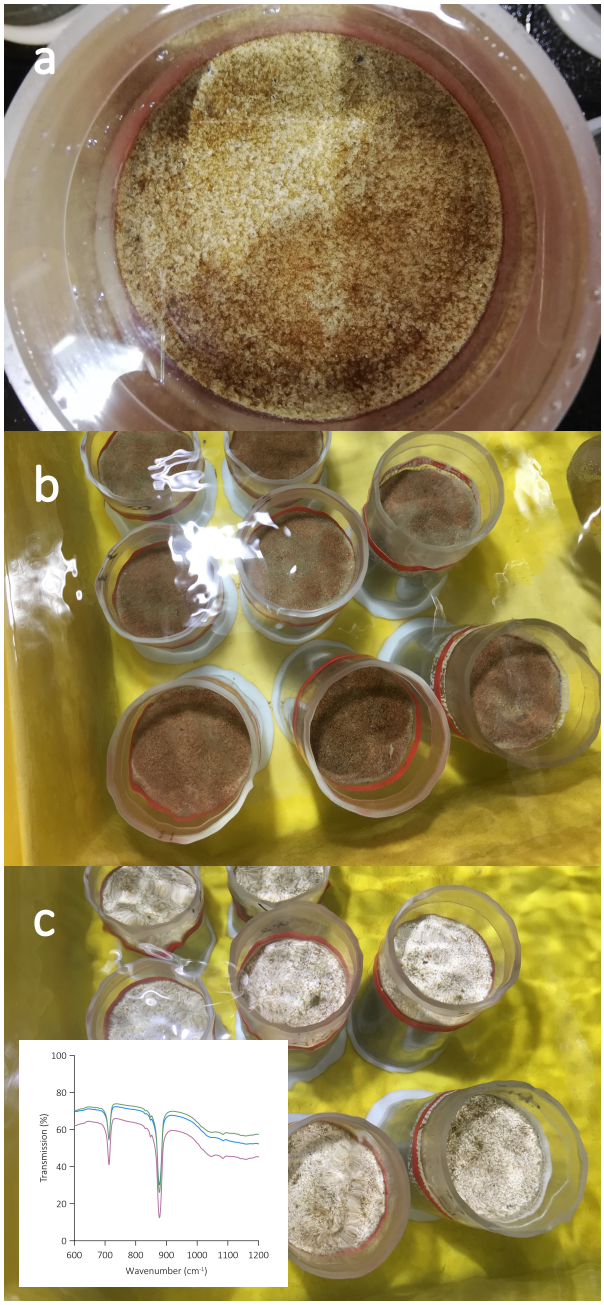

Figure 1 Photographs showing surfaces of intact cores of the subtidal silt sediment submerged in natural, recirculating seawater. The dark areas at the surface of the cores in (**a**) indicate the presence of pinnate diatoms. The cores in (**b, c**) received a 1-mm surface layers of (**b**) sterile carbonate free sand (Control) or (**c**) calcite (ground oyster shells; Treatment). Insert: Three replicate Fourier Transform Infrared (FTIR) spectra of ground oyster shell granules. The absorption observed around 877 and 713 cm^{-1} are due to vibrations of the carbon–oxygen double bond in the carbonate ion of calcite.

104 To assess the response of our subtidal silt sediment, we submerged 12 intact sediment cores
105 (Fig. 1) in each of two experimental units circulating natural seawater at *in situ* temperature
106 (Table 1) and provided 12 hours per day of photosynthetically active radiation to the
107 sediment surface at a flux density similar to that measured midday at the 10 m-deep core
108 collection site. We then deposited a 1 mm layer of <125 µm sterile particles of sand (six
109 cores, Control) or ground oyster shell (six cores, Treatment, Fig. 1c) onto the sediment
110 surface in each unit. Starting on day 2 of the 21-day experiment (Fig. S1), we gradually (0.04
111 pH units per day) increased the seawater $[H^+]$ in one of the experimental units using CO_2-
112 enriched air from pH 8.0 (pCO_2 = 472 µatm) to 7.6 (pCO_2 = 1216 µatm, Table 1) and then,
113 starting on day 16, measured vertical microprofiles of pH and $[O_2]$ under conditions of light
114 and darkness in individual cores (Fig. S1).

115

116 **Table 1** Properties of ambient and CO_2 enriched seawater (Mean ± 1SD). Temperature (°C) and salinity
117 are averages of 22 daily measurements whereas DIC and TA (µmol kg SW^{-1}) are averages of five
118 measurements taken during the final 10 days of the experiment. Seawater pH (total scale), $[H^+]$ (nmol
119 L^{-1}), pCO_2 (µatm), $[CO_3^{2-}]$ (µmol kg SW^{-1}), Ω_{CA} and Ω_{AR} were derived from the measured parameter for
120 a temperature of 15 °C.

121

	Ambient	CO_2 enriched
Measured parameters		
Temperature	14.6 ± 0.15	14.7 ± 0.16
Salinity	34.5 ± 0.07	34.5 ± 0.06
DIC	2112 ± 5	2261 ± 13
TA	2302 ± 10	2314 ± 10
Calculated parameters at 15 °C		
pH_T	7.99 ± 0.01	7.62 ± 0.03
$[H^+]$	10.3 ± 0.2	23.6 ± 0.9
pCO_2	472 ± 7	1216 ± 88
$[CO_3^{2-}]$	139 ± 3	66 ± 4
Ω_{CA}	3.32 ± 0.06	1.57 ± 0.09
Ω_{AR}	2.13 ± 0.04	1.01 ± 0.06

122

Results

Diel oscillations in porewater [H^+] and [O_2] at ambient pCO_2

Porewater microprofiles measured in the Control sediment cores revealed that the photosynthetically induced diel oscillations in porewater [H^+] and [O_2] extended to depths of about 8 mm (Figs 2 & 3). Integrated over the experimental 12/12 h light–dark cycle, the subtidal sediment was a sink for H^+ and a source of O_2. The [H^+] gradients in the diffusive boundary layer of the sediment indicated that, on average, the silt removed 2.5 times more H^+ from the overlying seawater in light than it released in darkness (Table 2, H^+ $flux_{DBL}$).

Table 2 Effects of seawater CO_2 enrichment and calcite deposit on the silt's average (± 1 SD) O_2 consumption, porewater oxygenation, and H^+ flux. O_2-pd, O_2 penetration depth (mm); DOE, diffusive O_2 exchange (µmol m^{-2} h^{-1}); R_A, depth-integrated O_2 production (µmol m^{-2} h^{-1}); R_V, integrated volume-specific O_2 consumption (= R_A/O_2-pd, nmol cm^{-3} h^{-1}). H^+ $flux_{DBL}$ and H^+ $flux_{sub}$ (mmol m^{-2} h^{-1}). Diffusive H^+ flux calculated from the vertical [H^+] gradients in the diffusive boundary layer and below the silt surface, respectively. Negative and positive DOU or *R* and H^+ flux values indicate sediment O_2 uptake and release, respectively. Numbers in parenthesis are number of replicate measurements (cores).

	Sand (Control)				Calcite (Treatment)			
	8.0	7.6	*d* ES	CI	8.0	7.6	*d* ES	CI
Light	(6)	(6)			(6)	(6)		
O_2-pd	8.5 ± 0.2	8.2 ± 0.7	0.56	0.28/0.83	9.0 ± 0.4	8.4 ± 0.4	1.56	1.36/1.75
DOE	489 ± 442	382 ± 277	0.32	-190/191	478 ± 342	490 ± 337	-0.04	-175/175
R_A	332 ± 247	315 ± 290	0.07	-143/143	302 ± 198	377 ± 333	-0.30	-142/141
	(5)	(5)			(5)	(6)		
H^+ $flux_{DBL}$	-217 ± 55	-437 ± 220	1.53	-87.3/90.4	-156 ± 92	-421 ± 140	2.41	-62.5/67.3
H^+ $flux_{sub}$	96 ± 16	42 ± 19	3.42	-6.4/13.2	121 ± 17	84 ± 3	3.51	-2.78/9.79
Darkness	(6)	(5)			(6)	(6)		
O_2-pd	7.6 ± 0.5	7.0 ± 0.7	1.32	1.04/1.60	7.8 ± 0.6	7.3 ± 0.6	0.97	0.66/1.28
DOE	-263 ± 52	-293 ± 55	0.60	-28.0/29.2	-178 ± 64	-239 ± 33	1.31	-25.1/27.7
R_A	-229 ± 14	-254 ± 53	0.73	-19.0/20.4	-219 ± 38	-235 ± 36	0.47	-18.5/19.4
R_V	-30 ± 2.2	-37 ± 9.6	1.20	-2.32/4.72	-28 ± 7.0	-32 ± 6.9	0.65	-2.93/4.23
	(4)	(4)			(6)	(6)		
H^+ $flux_{DBL}$	87 ± 46	152 ± 92	-0.97	-47.0/45.0	106 ± 90	-155 ± 111	2.83	-49.4/55.1
H^+ $flux_{sub}$	55 ± 21	41 ± 12	0.94	-9.2/11.1	84 ± 20	95 ± 33	-0.44	-14.6/13.7

Photosynthesis at the sediment surface lowered the [H^+] in the top millimetre of the sediment below that measured in the overlying seawater (Fig. 2a). This reversed the direction of the sediment–seawater H^+ exchange observed in darkness and increased the flux of H^+

from the bottom of the oxic zone to the surface sediment by a factor of 1.7 (H^+ $flux_{sub}$ in Table 2).

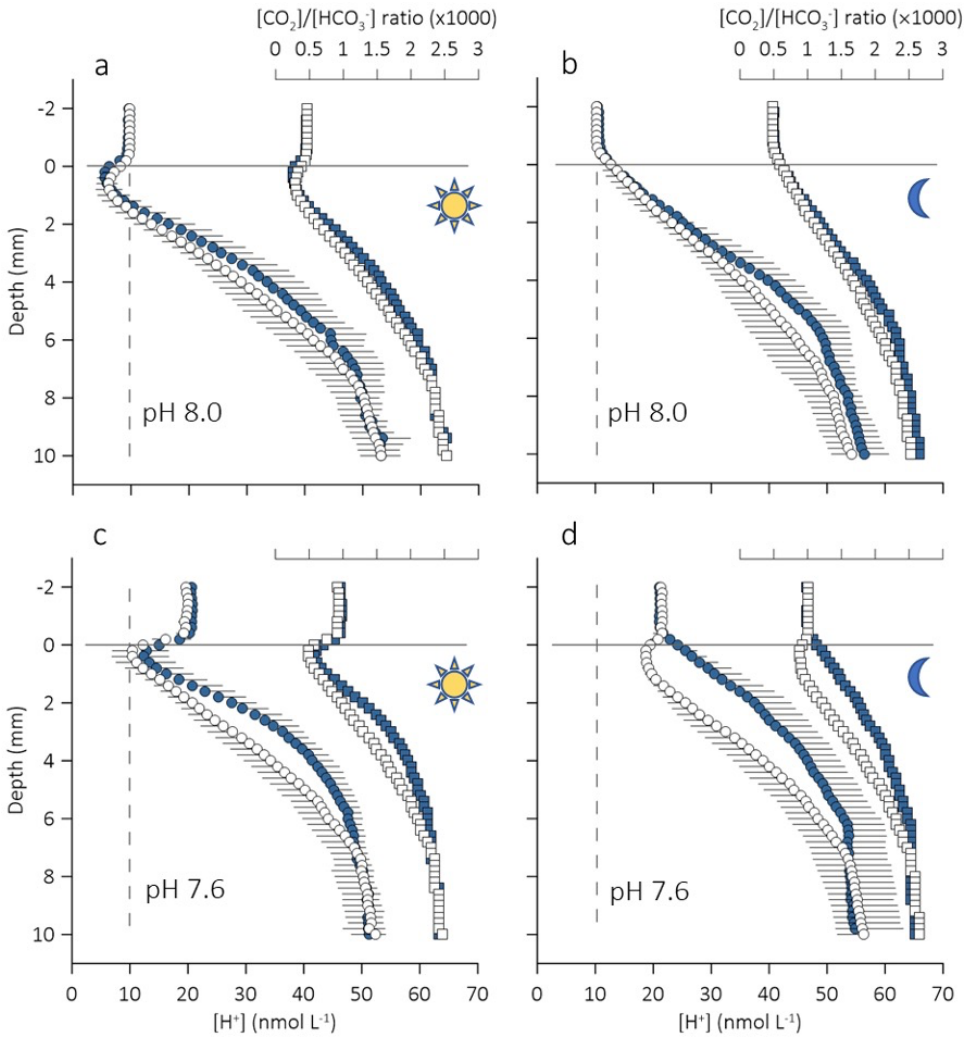

Figure 2 Average (n = 5) vertical microprofiles of porewater [H^+] (open and filled circles) measured in intact cores of subtidal silt submerged in (**a**, **b**) ambient seawater and (**c**, **d**) CO_2-enriched seawater under conditions of (**a**, **c**) light and (**b**, **d**) darkness. CO_2:HCO_3^- activity ratios (open and filled squares) presented alongside porewater [H^+] data were calculated in PHREEQC 3.0. A 1 mm surface layer of either sterile sand (blue symbols) or calcite (open symbols) was added to the sediment cores at the start of the experiment. The grey dashed and solid lines indicate the [H^+] in ambient seawater and the position of the sediment surface, respectively. Black horizontal lines extending to the right or left of the symbols indicate 1 SD.

Vertical [O_2] microprofiles measured in the diffusive boundary layer to compute the diffusive sediment–seawater O_2 exchange (DOE), and in the sediment porewater to compute the depth-integrated sediment O_2 production (R_A) showed that the Control released on average

160 1.9 and 1.4 times, respectively, more O_2 in light than it consumed O_2 in darkness (Table 2).
161 Note the large standard deviation of the average DOE measured in light indicating patchiness
162 in the distribution of benthic microphytes (Fig. 1a). In darkness, O_2 diffused from the
163 sediment overlying seawater to an average sediment depth of 7.6 mm (Fig. 3b). As expected,
164 photosynthesis at the surface of the sediment supersaturated the porewater of the top 2 mm
165 of the sediment with O_2, reversing the dark O_2 flux and increasing the O_2 penetration by 0.9
166 mm (Fig. 3a). Note that across the entire set of experimental treatment, DOE and R_A were
167 linearly correlated (R^2 = 0.96) but agreement between these two estimates gradually
168 decreased with increasing O_2 production (Fig. S2).

169

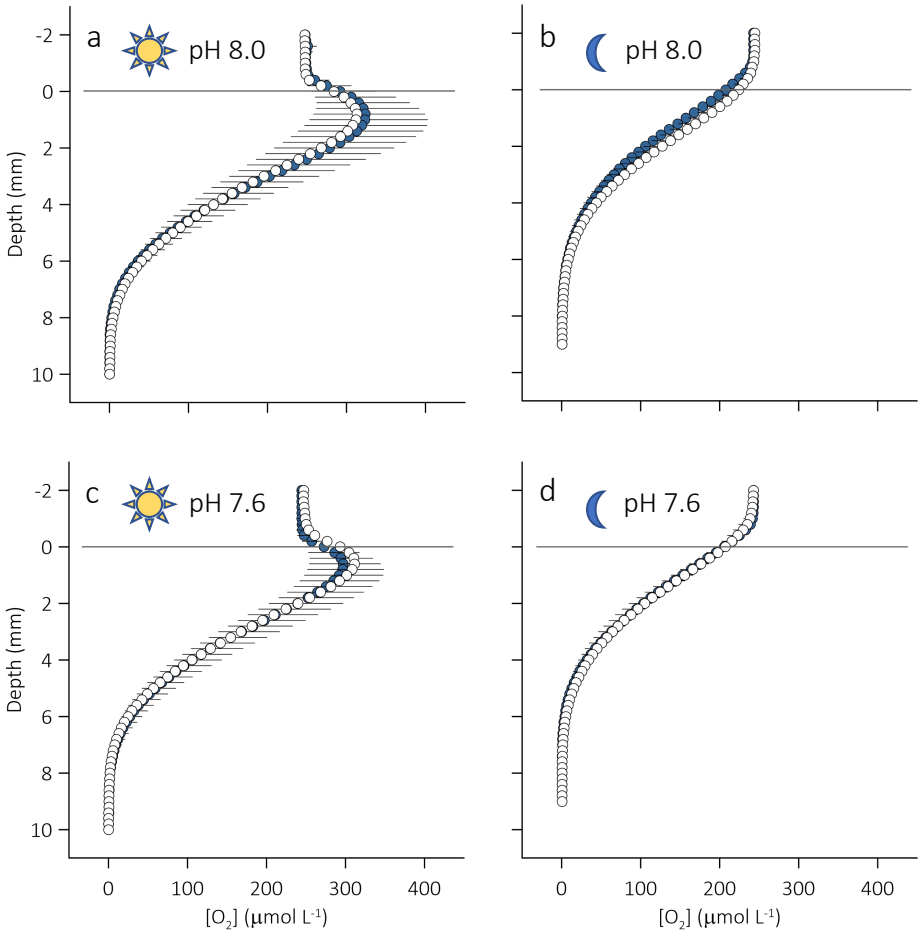

170

171 **Figure 3** Average (n = 6) vertical microprofiles of porewater [O_2] measured in intact cores of subtidal
172 silt submerged in (**a**, **b**) ambient seawater and (**c**, **d**) CO_2-enriched seawater under conditions of (**a**, **c**)
173 light and (**b**, **d**) darkness. A 1 mm surface layer of either sterile sand (blue symbols) or calcite (open
174 symbols) was added to the sediment cores at the start of the experiment. The grey horizontal lines
175 indicate the position of the sediment surface. Black horizontal lines extending to the right or left of
176 the symbols indicate 1 SD.

177

178 *Effects of calcite deposition*

179 In light, the flux of H^+ from the bottom of the oxic sediment layer into the calcite surface
180 layer (Treatment, H^+ $flux_{sub}$) exceeded that into the sand surface layer (Control) by factors of
181 1.3 and 2.0 in ambient and CO_2-enriched seawater, respectively (Tables 2, 3; Figure 2a, c).
182 Similarly, in darkness, the flux of H^+ from the bottom of the oxic sediment layer of the
183 Treatment exceeded that from the bottom of the oxic layer of the Control by factors of 1.5
184 and 2.3 in ambient and CO_2-enriched seawater, respectively (Tables 2, 3; Fig. 2b, c). The
185 calcite surface layer had no statistically clear effect on the H^+ flux across the diffusive
186 boundary layer (DBL) (H^+ $flux_{DBL}$, Table 2) except in darkness in CO_2-enriched seawater. Under
187 these conditions, the calcite layer resulted in a H^+ flux similar in size but opposite in direction
188 of that in the Control (152 ± 98 versus -155 ± 111 mmol m^{-2} h^{-1}, Table 2).

189 The [O_2] gradients in the sediment's diffusive boundary layer indicate that, in darkness, the
190 calcite Treatment removed on average less O_2 from the overlying seawater than the sand
191 control (DOE in Tables 2, 3). Inspection of the average microprofiles shown in Figure 3,
192 however, confirms this only for sediment in ambient seawater (Fig. 3b), but not for the
193 sediment in carbonated seawater (Fig. 3d). Furthermore, the estimates of R_A and the volume
194 specific O_2 production, R_V, which are based on the measured porewater microprofiles, do not
195 confirm that Control and Treatment differ in their O_2 demand (Tables 2, 3).

196 *Effects of seawater carbonation*

197 In light, the Control and Treatment removed H^+ from the overlying carbonated seawater (H^+
198 $flux_{DBL}$) at a larger rate than from the ambient seawater (Tables 2, 3; Fig. 2 a, c). As expected,
199 a greater H^+ uptake from the carbonated seawater was accompanied with smaller flux (H^+
200 $flux_{sub}$) from the bottom of the oxic layer (Tables 2, 3). Note that the increase in H^+ uptake
201 from the carbonated seawater outweighed the decrease in flux from the bottom of the oxic
202 sediment layer. That is, in light, the surface layers of Control and Treatment consumed more
203 H^+ in carbonated seawater than in ambient seawater.

204 In darkness, the flux of H^+ across the DBL of the Control sediment was independent of the
205 seawater pCO_2 (Tables 2, 3; Fig. 2 b, d). The H^+ flux across the DBL of the Treatment
206 sediment, on the other hand, indicated H^+ release in ambient seawater but uptake in
207 carbonated seawater.

Seawater carbonation also affected the O_2 penetration depth (O_2-pd); O_2 penetrated the Control and Treatment less from the carbonated seawater than from the ambient seawater, under both light and darkness (Tables 2, 3). The effects of seawater carbonation on the volume specific sediment O_2 consumption, R_V, and the DOE measured in darkness were statistically not clear.

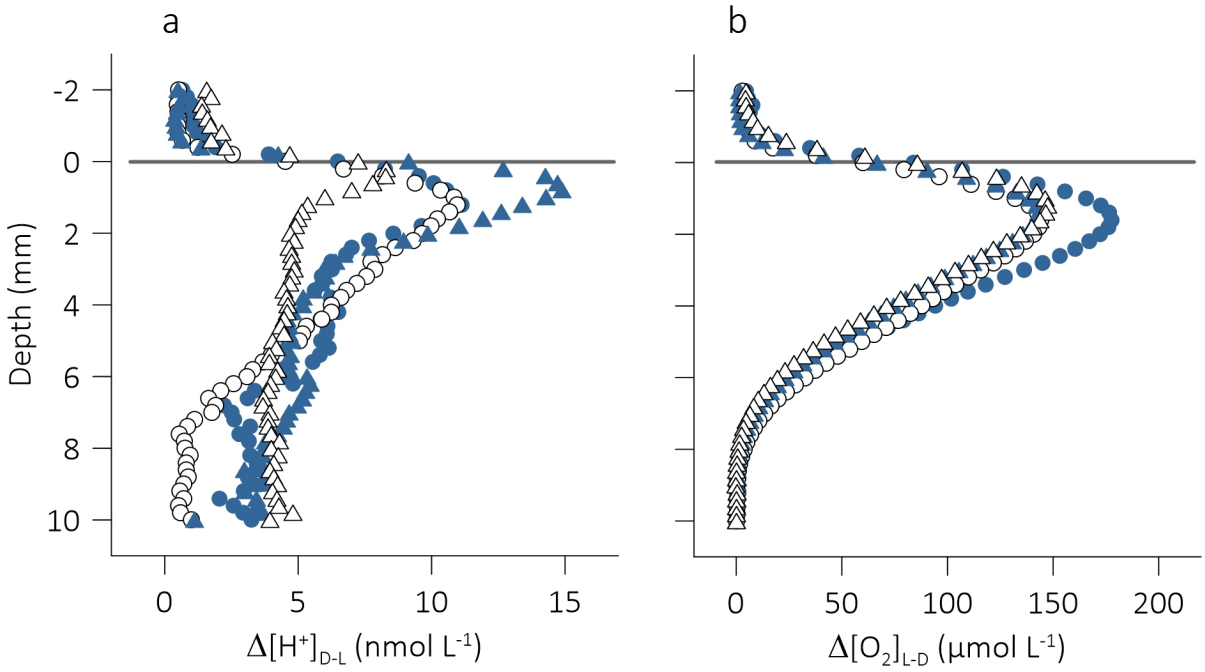

Figure 4 Diel oscillations in porewater (**a**) $[H^+]$ ($\Delta[H^+]_{D\text{-}L}$, nmol L^{-1}) and (**b**) $[O_2]$ ($\Delta[O_2]_{L\text{-}D}$, µmol L^{-1}) as a function of depth in the surface layer of intact cores of subtidal silt sediment submerged in ambient (circles) and CO_2-enriched (triangles) seawater. A 1 mm surface layer of either sterile sand (filled symbols) or calcite (open symbols) was added to the sediment cores. The horizontal grey line indicates the position of the sediment surface.

Discussion

Our measurements in cores of photosynthetic subtidal silt sediment with 1 mm of added sterile sand (Control) revealed that carbonation of the overlying seawater increases the peak-to-peak amplitude of the diel porewater $[H^+]$ oscillations (Fig. 4a, compare filled vs open triangles). Two effects likely contribute to this increase: (1) in darkness, sedimentary microbial reaction processes seem to amplify the positive effect of seawater carbonation on porewater $[H^+]$ (Fig. 5a, filled symbols), and (2) replenishment of the CO_2 taken up during photosynthesis by the bicarbonate pool consumes H^+ at a greater rate in carbonated seawater than in ambient seawater (Fig. 5a, open symbols). Furthermore, we showed that

seawater carbonation decreased the sediment penetration of O_2 in both light and darkness (Tables 2, 3) suggesting a CO_2 response of microbial reaction processes that either directly or indirectly consume O_2.

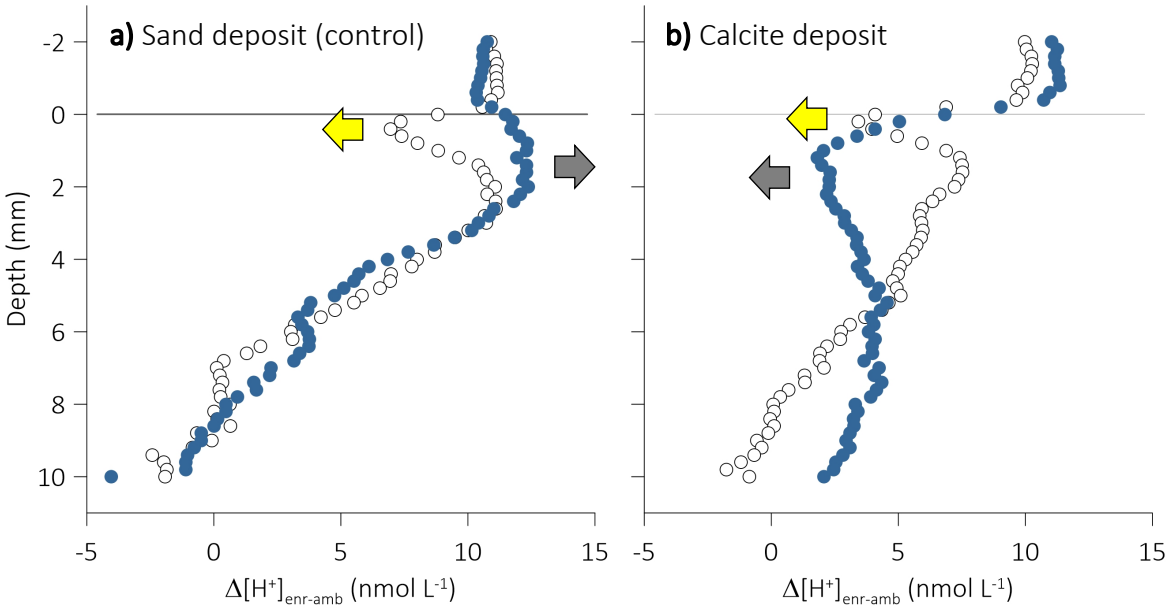

Figure 5 Effect of seawater CO_2 enrichment on the sediment porewater $[H^+]$ ($\Delta[H^+]_{enr\text{-}amb}$, nmol L^{-1}) under conditions of light (open symbols; yellow arrow) and darkness (closed symbols; shaded arrow) and added (**a**) sterile sand (Control) or (**b**) calcite (Treatment).

The addition of biogenic calcite to the surface of the sediment increased the flux of H^+ from the bottom of the oxic sediment layer (H^+ $flux_{sub}$) towards the sediment surface, in light and darkness, and in both ambient and carbonated seawater (Tables 2, 3). We suspect that this was caused by dissolution of calcite at the sediment-facing boundary of the calcite deposit. (note that the statistically clear effect of seawater pCO_2 on this flux—a decrease observed only in light (Tables 2, 3)—was caused by an increase in the supply of H^+ across the DBL following the carbonation of the seawater). The H^+ flux across the seawater-facing boundary of the calcite deposit (H^+ $flux_{DBL}$), on the other hand, did statistically not differ from the flux across the diffusive boundary of the Control, except in carbonated seawater under conditions of darkness (Tables 2, 3). Under these conditions, seawater carbonation decreased the efflux of H^+ from the sediment and so raised the porewater $[H^+]$ sufficiently to trigger calcite dissolution across the entire deposit. This dissolution then decreased the porewater $[H^+]$ below that in the CO_2-enriched overlying seawater reversing the direction of the H^+ flux (Fig.

2d). Consequently, the peak-to-peak amplitude of the diel porewater $[H^+]$ oscillations decreased (Fig. 4a, open triangles). Such an effect was not observed in ambient seawater: the overlapping $\Delta[H^+]_{D\text{-}L}$ profiles in Figure 4a (open and closed circles) indicate that in ambient seawater, the influences of photosynthesis on $[H^+]$ in the porewater of Control and Treatment were similar. That is, in ambient seawater, the addition of calcite did not alter the photosynthetically induced $[H^+]$ oscillations.

Besides differences between Control and Treatment in the flux of H^+ from the bottom of the oxic sediment layer, the O_2 gradients in the diffusive boundary layer measured in darkness under conditions of ambient and carbonated seawater revealed differences between Control and Treatment in the diffusive O_2 exchange (DOE, Tables 2, 3). These gradients may not correctly reflect the steady-state sediment–seawater O_2 exchange, but if so, then the Treatment seemed to have removed less O_2 from its overlying seawater than the Control in both ambient (*d* ES = -1.6) and carbonated seawater (*d* ES = -1.35). We note, however, that the proxies derived from the measured porewater $[O_2]$ profiles (O_2-pd, R_A and R_V) did not return statistically clear differences.

We posit that the observed increase in the flux of H^+ from the bottom of the oxic layer of the Treatment sediment resulted from the dissolution of the sediment-facing boundary of the calcite deposit. Inspection of the $[H^+]$ microprofiles shown in Figure 2b reveals that this may have started at a porewater $[H^+]$ of 15–20 nmol L^{-1} (pH 7.8–7.7)—the concentrations measured at 1 mm depth. We can infer from the Control that carbonation of the sediment-overlying seawater then raised the $[H^+]$ in the porewater of the calcite layer above ~25 nmol L^{-1} (below pH 7.6, Fig. 2d, Control) initiating dissolution, which lowered the porewater $[H^+]$ to about 20 nmol L^{-1} (increased pH to ~7.7) as shown in Figure 2d. If the dissolution–precipitation balance was to shift toward net dissolution at $\Omega_{CA} < 0.7$ (Subhas et al. 2017), and assuming that porewater total alkalinity, TA = 2.3 mmol kg^{-1}, then calcite should be stable at pH > 7.25, and the $[H^+]$ profiles across the calcite layer should resemble the profiles measured in the Control. Our results suggest that dissolution started at a much lower $[H^+]$ (higher pH) confirming the evidence presented by others (Ries et al. 2016) who have observed that gross dissolution of whole-shell biogenic $CaCO_3$ occurred in treatments that were oversaturated ($\Omega > 1$) with respect to calcite. The abundance of large motile pennate diatoms (species of the genera *Pleurosigma*, *Gyrosigma*, *Nitzschia*, *Thalassionema*, and

Bacillaria) raises the possibility that the dissolution of the surface calcite was enhanced by the activity of extracellular enzymes. Diatoms use an extracellular carbonic anhydrase (Nimer et al. 1999, Hopkinson et al. 2013), located in the periplasmatic space (Tachibana et al. 2011, Samukawa et al. 2014), as part of a carbon-concentrating mechanism that increases the flux of CO_2 towards the carboxylating enzyme, ribulose-1,5-bisphosphate carboxylase-oxygenase (RubisCO) (Matsuda et al. 2017). This enzyme catalyses the otherwise slow inter-conversion of CO_2 and HCO_3^- and in this case, facilitates CO_2 uptake by generating CO_2 from HCO_3^- at the cell surface (Hopkinson et al. 2013) through a two-step process, a hydration–dehydration step followed by a rate-limiting transfer of protons, which is presumable buffered by the acidic polymerised silica of the diatoms' cell wall (Milligan & Morel 2002). Evidence presented by Subhas et al. (2017) suggests this activity increases calcite dissolution across all saturation states, the effect being most pronounced close to equilibrium ($\Omega_{CA} = 1$).

What amplified the effects of biogeochemical processes on porewater [H^+] in carbonated seawater?

In Figure 5, we use vertical $\Delta[H^+]_{enr\text{-}amb}$ profiles to assess how seawater carbonation altered [H^+] in both the sediment-overlying seawater and the sediment porewater. As mentioned above, for both, Control and Treatment, injection of CO_2-enriched air will initially have decreased the porewater–seawater [H^+] gradient observed in darkness and so the dark H^+ efflux. If sedimentary reaction processes kept producing and consuming H^+ at unchanged rates, then the porewater [H^+] and sediment–seawater H^+ efflux must have gradually increased until net production and efflux were again in equilibrium. That is, the [H^+] at the sediment surface must have increased by as much as the [H^+] in the bottom seawater and $\Delta[H^+]_{enr\text{-}amb}$ would gradually be attenuated with sediment depth. However, Figure 5a shows that in darkness, $\Delta[H^+]_{enr\text{-}amb}$ in the porewater of the upper 2 mm of the sediment exceeded that in the overlying seawater. This suggests that net-production of H^+ had increased leading to higher porewater concentrations and a higher H^+ efflux. The average H^+ efflux measured in CO_2-enriched seawater was in fact higher than that measured in ambient seawater (*d* ES = –0.97, Table 2), but this difference was statistically not clear (Table 3, post-hoc $p = 0.7611$).

311 **Table 3** Summary of two-way ANOVA *p* values in light and darkness testing for the effects of seawater
312 pCO_2 (ambient (amb), enriched (enr)) and sediment surface deposit (sand (san), calcite (cal)) on the
313 silt's O_2 penetration depth (O_2-pd), diffusive O_2 exchange (DOE), depth integrated O_2 consumption
314 (R_A), depth integrated volume specific O_2 consumption, R_V, H^+ fluxes across the diffusive boundary
315 layer (H^+_{DBL}) and at the bottom of the oxic sediment layer (H^+_{sub}).

316

	pCO_2	Deposit	pCO_2 × Deposit	*Tukey post-hoc test results*
A) Light				
O_2-pd	0.0428	0.2724	0.7552	
DOE	0.8116	0.7366	0.9599	
R_A	0.9551	0.7946	0.7127	
H^+ $flux_{DBL}$	0.0128	0.7591	0.2052	
H^+ $flux_{sub}$	0.0029	<0.0001	0.1100	
B) Darkness				
O_2-pd	0.0235	0.3716	0.8350	
DOE	0.0532	0.0048	0.4776	
R_A	0.2498	0.4024	0.8026	
R_V	0.0883	0.3647	0.6326	
H^+ $flux_{DBL}$	0.0335	0.0036	0.0014	amb: san vs cal, p = 0.9887; enr: san vs cal, p = 0.0007 san: amb vs enr, p = 0.7611; cal: amb vs enr, p = 0.0010
H^+ $flux_{sub}$	0.8980	0.0017	0.2787	

317

318 Following Middelburg et al. (2020), the instantaneous effect of a biogeochemical process on
319 $[H^+]$ is the product of the net charge exchanged during the process (Δcharge), the sensitivity
320 factor of seawater ($\delta pH/\delta CBA$), and the process intensity $I_{process}$ (mol m^{-3} s^{-1}):

321 $$dpH = \Delta\text{charge} \times \left(\frac{\partial pH}{\partial CBA}\right) \times I_{process} \quad (1)$$

322 Because the sensitivity factor and the net charge exchange are functions of pH, the influence
323 of a biogeochemical process also depends on pH. In other words, the carbonation-induced
324 acidification of the sediment porewater can alter the positive or negative effect of
325 biogeochemical reaction processes on porewater $[H^+]$ even if the intensity of the reaction
326 process remains unchanged. For aerobic mineralisation and the reoxidation of reduced
327 solutes with O_2, this pH dependency sees the production of $[H^+]$ steeply increasing as
328 porewater $[H^+]$ increases above 10 nmol L^{-1} (pH decreases below 8.0, Soetaert et al. 2007).
329 That is, an increase in porewater $[H^+]$ will have increased the production of H^+ by porewater
330 microbial reaction processes raising $\Delta[H^+]_{enr\text{-}amb}$ above that observed in the overlying
331 seawater, even if the reaction process intensity remained unchanged. It would follow then

that the observed increase in $\Delta[H^+]_{enr\text{-}amb}$ does not necessarily imply that an ecosystem process has responded to additional CO_2 (ecosystem feedback).

While in darkness $\Delta[H^+]_{enr\text{-}amb}$ in the porewater of the Control exceeded that in the overlying seawater, in light, it steeply decreased below that in the overlying seawater reaching a minimum just below the sediment surface (Fig. 5a). This suggests photosynthesis must have removed more H^+ in carbonated seawater than in ambient seawater. Again, this may have followed from the pH dependencies of the seawater sensitivity factor and the net charge exchange (see above); Soetaert et al. (2007) showed that the consumption of porewater H^+ by photosynthesis based on ammonium or nitrate increases steeply as the environmental $[H^+]$ increases above 10 nmol L^{-1}. An increase in the process intensity, that is, CO_2-enhanced photosynthetic carbon fixation, on the other hand, should be reflected in the measured $[O_2]$ microprofiles showing an increase in O_2-pd and sediment–seawater O_2 release. There is, however, no evidence for such effect (Figs 3b, 4 a, c, Table 2). None of the $[O_2]$ microprofiles and O_2 production estimates indicate a greater net production of O_2 in carbonated seawater.

Besides enhancing the H^+ production (dark) and consumption (light) in the porewater of the surface sediment, seawater carbonation caused a statistically clear decrease in O_2-penetration depth (O_2-pd, *d* ES 1.3), and, although statistically not clear, an increase in the average integrated volume-specific O_2 consumption (R_V, Control, *d* ES = 1.2). The latter effect and the elevated $\Delta[H^+]_{enr\text{-}amb}$ may have a common cause, a positive CO_2 response of microbial reaction processes that generate H^+ *and* consume O_2: the microbial reoxidation of reduced solutes (iron, manganese and sulphur) with O_2 and aerobic mineralisation and nitrification. For example, an increase in the production and subsequent oxidation of Fe^{2+} would have raised both the O_2 demand and the porewater $[H^+]$ in the surface sediment adding to the effects of pH-dependent sensitivity factor and net exchange of charge, as per Equation 2.

$$4Fe^{2+} + HCO_3^- + 10H_2O \rightarrow 7H^+ + 4Fe(OH)_3 + CH_2O \quad (2)$$

Here, for the first time, we presented evidence for a positive effect of seawater carbonation on the peak-to-peak amplitude of the dark–light oscillation in porewater $[H^+]$ that characterise cohesive photosynthetic sediment. We discussed possible causes of this effect and showed that dissolution of carbonate, if added to the surface, will diminish these oscillations. The pH dependencies of both the seawater sensitivity factor and the net

exchange of charge may explain why sediment biogeochemical processes in carbonated seawater added and removed more H^+ to and from the porewater in darkness and light, respectively, than they did in ambient seawater. Ecosystem feedback in the form of CO_2-induced changes in the intensity of photosynthesis in light and respiration in darkness may also explain an enhanced consumption and production, respectively, of porewater H^+, but this is not consistent with the observed decrease in O_2 penetration in light and the similarity of the [O_2] microprofiles measured in ambient and carbonated seawater. One possible process that explains this discrepancy is increased microbial reoxidation of reduced solutes with O_2, and thus increased sediment O_2 demand, decreasing the O_2 penetration while increasing porewater [H^+]. The dissolution of the added calcite then effectively countered the increase in porewater [H^+] (Fig. 5b), but not the CO_2-induced decrease in O_2 penetration. This dissolution should not be considered as ecosystem feedback because calcite was not naturally present at the sediment surface. It indicates, however, a challenge for recruits of calcifying fauna arriving at the sediment surface. A chemically more aggressive (acidified) surface layer may prevent recruitment and so alter animal-generated spatial and temporal heterogeneities in the sediment (see, e.g., Zhu et al. 2006).

Material and Methods

Sediment collection and properties

On June 11th 2019, we collected 24 cores of subtidal silt with SCUBA at 10 m water depth in Man O'War Bay (S 36° 47' 38", E 175° 10' 14"), Hauraki Gulf, New Zealand, as described in Vopel et al. (2018, 2021). The cores were kept below 15 °C, the *in situ* seawater temperature, during a 2.5 h trip to the laboratory. The salinity of the seawater was 34.5. Loss of weight of the silt's upper 10 mm layer after drying at 60 °C and combustion at 550 °C indicated that on average, porewater accounted for 68 ± 1.3 % of the silt's wet weight, and that 9.5 ± 0.4 % of the silt's dry weight (± 1 SD, n = 3) was organic matter. The calcium carbonate content of the upper 10 mm of the sediment was 4.1 ± 0.2 % dry weight (n = 3). Chlorophyll *a* and phaeopigment contents were 12.5 ± 1.9 and 20.5 ± 2.4 µg (g dry weight)$^{-1}$ (n = 3) giving a Chl *a*/phaeopigment ratio of 0.6. Particle sizes, determined using ~10 mL sample of the homogenized silt and a Malvern Mastersizer 2000, ranged from 0.24 to 350 µm with a volume weighted mean of 35.7 ± 0.9 µm (Kurtosis: 8.0 ± 1.3, Skewness: 2.6 ± 0.2).

Laboratory setup and seawater properties

We submerged 12 randomly selected sediment cores in two independent experimental units (EU) each circulating ~1120 L of natural seawater (Table 2). Details of these units are described in Vopel et al. (2018, 2021). LED floodlights provided ~130 µmol quanta m^{-2} s^{-1} of photosynthetically active radiation (PAR) from 7 am to 7 pm at the surface of the submerged sediment cores. This intensity was similar to that measured midday at the core collection site (K Vopel unpublished data). Starting on d 2 of the experiment, we carbonated the seawater circulating in one EU by automatic stepwise injection of CO_2-enriched air (5% CO_2, 21% O_2 in nitrogen) to decrease its pH by 0.04 units per day (for 10 d) until a pH of 7.60 was reached (Fig. S1). The seawater pH was then maintained at 7.60 for a further 9 d until the end of the experiment (d 21). The level of carbonation was controlled by CapCtr software (Loligo Systems Aps), a SenTix HWD electrode connected to a pH 3310 meter (WTW), and a solenoid valve. For additional details including the calibration of pH electrodes see Vopel et al. (2018).

We measured the seawater salinity daily and kept it between 34.4 and 34.7 by adding ultrapure water. One litre of seawater collected from each EU weekly was analysed for dissolve inorganic carbon (DIC) by coulometry and total alkalinity (TA) by potentiometric titration following the SOP's 2 and 3a procedures (Dickson et al. 2007). D. Pierrot's adaptation of the CO_2Sys.BAS program (Lewis and Wallace 1998) computed the seawater pCO_2 and pH (seawater scale, mol kg-SW^{-1}). The dissociation constant for HSO_4^- was taken from Dickson (1990); the values of K_1 and K_2 of carbonic acid were from Mehrbach et al. (1973) refitted by Dickson and Millero (1987). The CO_2Sys.BAS computations confirmed that the stepwise increase in the injection of CO_2-enriched air increased the seawater pCO_2 by a factor of ~2.6 and decreased seawater pH from 8.0 to 7.6 (Table 1).

Sediment treatment

On d 1 of the experiment, we added a 1 mm thick surface layer of biogenic calcite (Fig. 1) to six cores in each of the two experimental units. To do so, we briefly ground (Omni Ruptor 4000 Ultrasonic Homogenizer) bleach sterilised and rinsed oyster shells and sieved the material to exclude particles >125 µm. Fourier transform infrared spectroscopy of this material confirmed the identity of the $CaCO_3$ mineral (Fig. 1). We weighed 2 g into each of 12 seawater-filled 100-mm diameter petri-dishes to create a consistent, 1 mm thick layer at the

422 bottom of each petri dish. The contents of each petri dish was then frozen at -80 °C and one
423 of the resulting solid seawater/calcite disks was placed into the headwater space of each
424 core. As the disks thawed, an even layer of calcite was distributed onto the surfaces of the
425 sediment cores. To avoid disturbing the settling particles, the cores were isolated from the
426 surrounding seawater until the surface layers of calcite had formed (~20 min). A 1 mm thick
427 surface layer of sand particles was added to each of the remaining cores as a control using
428 the same technique. The sand particles were first heated for 4 h at 550 °C to remove organic
429 carbon and then sieved to exclude particles >125 µm. After sieving, they were heated for a
430 second time for 1 h at 840 °C to remove $CaCO_3$.

431 ## O_2 and pH microprofiling

432 Starting on d 16 (i.e. after 4 d at pH = 7.6 in the enriched treatments, Fig. S1) of the
433 experiment, we recorded one vertical [O_2] and pH microprofile in each core under conditions
434 of darkness and light. Measurements were made after at least 6 h exposure to light or
435 darkness and the cores were selected at random across the 5 d it took to complete all the
436 measurements. The vertical profiles were made at a 0.2 mm resolution starting from a
437 position 2 mm above the sediment surface into the anoxic sediment at 9–10 mm depth with
438 PreSens (optodes) and Unisense (pH microelectrodes, 100-µm tip) hard- and software. We
439 then used the section of an [O_2] or pH microprofile that described the diffusive boundary
440 layer of the sediment to calculate the diffusive O_2 (DOE, µmol m^{-2} h^{-1}) and H^+ (H^+ $flux_{DBL}$,
441 mmol m^{-2} h^{-1}) exchange, respectively. The molecular diffusion coefficients of O_2 and H^+ (D_0)
442 were from Broecker and Peng (1974) and Cussler (2009), respectively, and corrected for
443 temperature and salinity as described by Li and Gregory (1974).

444 The O_2 penetration depth (O_2-pd, mm) was defined as the depth at which the porewater [O_2]
445 decreased below 1 µmol L^{-1}. The sediment section of the [O_2] profiles was used to derive the
446 silt's areal, depth integrated O_2 consumption (R_A, µmol m^{-2} h^{-1}), and integrated volume-
447 specific O_2 consumption ($R_V = R_A/O_2$-pd, nmol cm^{-3} h^{-1}), with the model PROFILE (Berg et al.
448 1998) neglecting the sediment biodiffusivity and irrigation, and assuming a constant porosity,
449 $\phi = 0.85$. To derive the flux of H^+ from the deeper sediment (H^+ $flux_{sub}$, mmol m^{-2} h^{-1}), we use
450 a section of the [H^+] profile that described the bottom 2 mm of the oxic layer. The diffusivities
451 corrected for tortuosity were calculated as $D_S = D_0 \times \phi$, following Ullman and Aller (1982). The
452 difference in molecular diffusivity between the silt and the overlying seawater caused a

distinct change in the slope of the measured [O_2] profile at a position that marked the silt surface (Jørgensen and Revsbech 1985, Rasmussen and Jørgensen 1992).

Equilibrium speciation calculations

The equilibrium activity ratio of CO_2 to HCO_3^- is presented in Figure 2. Carbonate species distributions were determined in PHREEQC 3.0 using the seawater composition presented in Nordstom et al. (1979) to calculate the activity of associated inorganic complexes. Calculations were completed for each microprofile depth. While the total alkalinity in pore waters was not known, the activity ratio of CO_2:HCO_3 is independent of [DIC] and can be computed using the relevant equilibrium constants and the concentration of protons in solution.

Data analyses

The vertical profiles of $\Delta[H^+]_{L\text{-}D}$ and $\Delta[H^+]_{enr\text{-}amb}$ shown in Figures 4 and 5 were calculated using averages of [H^+] measured in replicate cores under conditions of light and darkness or in acidified and ambient seawater, respectively. We follow Dushoff et al. (2019) when describing the conclusion from our statistical tests in terms of statistical 'clarity' rather than 'significance'. We used separate two way analysis of variance (ANOVA) to test the treatment effects of seawater pCO_2 (ambient, enriched) and sediment surface deposit (sand control, calcite) and their interaction on O_2-pd, DOE, R_A, H^+ $flux_{DBL}$ and H^+ $flux_{sub}$ under light and dark conditions. When a clear pCO_2 × Deposit interaction was detected, separate Tukey HSD post-hoc analyses were undertaken for Deposit under pCO_2 conditions and vice versa. All statistical tests were conducted using Statistica (StatSoft GmbH). Prior to analysis, data were checked for normality and homogeneity of variance (visual inspection of residuals); no transformations were required. The *d* Effect Size (*d* ES) and 95% Confidence Interval were computed using the Excel routine created by Jared DeFife, Emory University, 2009 (web.cs.dal.ca/~anwar/ds/Exce;4.xlsx).

Data availability

The datasets are available from the corresponding author on reasonable request.

Acknowledgements

Evan Brown and Fabian Doeweler assisted in the field and the laboratory. Kim Currie analysed the seawater dissolved inorganic carbon content and total alkalinity. This research was supported by a Smart Ideas award (UOWX1602) from the New Zealand Ministry of Business, Innovation and Employment.

Author Contributions

K.V., A.M. and C.A.P. conceived the experiment. K.V., A.M. and S.B. performed the experiment. K.V. and C.A.P. analysed the data. A.H. analysed the crushed oyster shells. K.V. wrote the paper with assistance from C.A.P., A.M, A.H., C.K.L. and S.C.C.

Addition Information

Competing Interests: The authors declare no competing financial interests.

References

Berg PN, Risgaard-Petersen N, Rysgaard S. Interpretation of measured concentration profiles in sediment pore water. *Limnology & Oceanography* **43**, 1500–1510 (1998).

Borges, A. V., Gypens, N. Carbonate chemistry in the coastal zone responds more strongly to eutrophication than ocean acidification. *Limnology & Oceanography* **55**, 346–353 (2010)

Broecker WS, Peng T-H. Gas exchange rates between air and sea. *Tellus* **26**(1-2), 21–35 (1974).

Cai W-J, Hu X, Huang W-J, Murrell MC, Lehrter JC, Lohrenz SE, Chou W-C, Zhai W, Hollibaugh JT, Wang Y, Zhao P, Guo X, Gundersen K, Dai M, Gong G-C. Acidification of subsurface coastal waters enhanced by eutrophication. *Nature Geoscience* **4**, 766–770 (2011).

Clements JC, Hunt HL. Marine animal behaviour in a high CO_2 ocean. *Marine Ecology Progress Series* **536**, 259–279 (2015).

Clements, JC, Woodard KD, Hunt HL. Porewater acidification alters the burrowing behavior and post-settlement dispersal of juvenile soft-shell clams (*Mya arenaria*). *Journal of Experimental Marine Biology and Ecology* **477**, 103–111 (2016).

506 Cussler EL (2009) Diffusion: mass transfer in fluid systems. Cambridge University Press

507 Dickson AG, Millero FJ. A comparison of the equilibrium constants for the dissolution of
508 carbonic acid in seawater media. *Deep Sea Res* **34**(10), 1733–1743 (1987).

509 Dickson AG, Sabine CL, Christian JR. Guide to best practices for ocean CO_2 measurements:
510 PICES *Special Publication 3.* http://cdiac.ornl.gov/oceans/Handbook_2007.html (2007).

511 Dickson AG. Standard potential of the reaction: $AgCl_{(s)} + 12H_{2(g)} = Ag_{(s)} + HCL_{(aq)}$, and the
512 standard acidity constant of the ion HSO_4^- in synthetic sea water from 273.15 to 318.15
513 K. *The Journal of Chemical Thermodynamics* **22**, 113–127 (1990).

514 Dushoff J, Kain MP, Bolker BM. I can see clearly now: Reinterpreting statistical significance.
515 *Methods in Ecology and Evolution* **10**, 756–759 (2019).

516 Egleston ES, Sabine CL, Morel FMM. Revelle revisited: Buffer factors that quantify the
517 response of ocean chemistry to changes in DIC and alkalinity. *Global Biogeochem Cycles*
518 **24**, GB1002 (2010).

519 Frankignoulle M. A complete set of buffer factors for acid/base CO_2 system in seawater.
520 *Journal of Marine Systems* **5**, 111–118 (1994)

521 Hagens M, Slomp CP, Meysman FJR, Seitaj D, Harlay J, Borges AV, Middelburg JJ.
522 Biogeochemical processes and buffering capacity concurrently affect acidification in a
523 seasonally hypoxic coastal marine basin. *Biogeosciences* **12**, 1561–1583 (2015).

524 Hofmann, G. E., Smith, J. E., Johnson, K. S., Send, U., Levin, L. A., Micheli, F., Paytan, A., Price,
525 N. N., Peterson, B., Takeshita, Y., Matson P. G., Crook E. D., Kroeker K. J., Gambi M. C.,
526 Rivest E. B., Frieder C. A., Yu P. C., Martz T. R. High-frequency dynamics of ocean pH: A
527 multi-ecosystem comparison. *PLoS ONE* 6, e28983 (2011)

528 Hopkinson BM, Meile C, Shen C. Quantification of extracellular carbonic anhydrase activity in
529 two marine diatoms and investigation of its role. *Plant Physiol* **162**, 1142–1152 (2013)

530 Jørgensen BB, Revsbech NP. Diffusive boundary layers and the oxygen uptake of sediments
531 and detritus. *Limnology & Oceanography* **30**(1), 111–122 (1985).

532 Jury CP, Thomas FIM, Atkinson MJ, Toonen RJ. Buffer capacity, ecosystem feedbacks, and
533 seawater chemistry under global change. *Water* **5**, 1303–1325 (2013).

534 Lewis E, Wallace DWR. Program developed for CO_2 system calculations. ORNL/CDIAC-105.
535 Carbon Dioxide Information Analysis Center, Oak Ridge National Laboratory, U.S.
536 Department of Energy, Oak Ridge, Tennessee (1998).

537 Li Y-H, Gregory S. Diffusion of ions in sea water and in deep-sea sediments. *Geochim*
538 *Cosmochim Acta* **38**(5), 703–714 (1974).

539 Marinelli RL, Woodin SA. Experimental evidence for linkages between infaunal recruitment,
540 disturbance, and sediment surface chemistry. *Limnology and Oceanography* **47(1)**, 221–
541 229 (2002).

542 Matsuda Y, Hopkinson BM, Nakajima K, Dupont CL, Tsuji Y. Mechanisms of carbon dioxide
543 acquisition and CO_2 sensing in marine diatoms: a gateway to carbon metabolism.
544 *Philosophical Transactions of the Royal Society B* **372**, 20160403 (2017)

545 Mehrbach C, Culberson CH, Hawley JE, Pytkowicz RN. Measurement of the apparent
546 dissociation constants of carbonic acid in seawater at atmospheric pressure. *Limnology &*
547 *Oceanography* **18**, 897–907 (1973).

548 Middelburg JJ, Soetaert K, Hagens M. Ocean alkalinity, buffering and biogeochemical
549 processes. *Reviews of Geophysics* **58**, e2019RG000681 (2020).

550 Milligan AJ, Morel FMM. A proton buffering role for silica in diatoms. *Science* **297**, 1848–1850
551 (2002).

552 Nimer NA, Brownlee C, Merrett MJ. Extracellular carbonic anhydrase facilitates carbon
553 dioxide availability for photosynthesis in the marine dinoflagellate *Prorocentrum micans*.
554 *Plant Physiology* **120**, 105–112 (1999)

555 Nordstrom DK, Jenne EA, Ball JW. Redox equilibria of iron in acid mine waters. In Chemical
556 Modeling in Aqueous Systems (ed. Jenne EA). American Chemical Society Symposium
557 Series v. 93, Washington, DC: American Chemical Society, pp. 57–79 (1979)

558 Pawlik JR. Chemical ecology of the settlement of benthic marine invertebrates. *Oceangraphy*
559 *and Marine Biology: An Annual Review* **30**, 273–335 (1992).

560 Provoost, P., Heuven, S. van, Soetaert, K., Laane, R. W. P. M. & Middelburg, J. J. Seasonal and
561 long-term changes in pH in the Dutch coastal zone. *Biogeosciences* **7**, 3869–3878 (2010).

562 Rasmussen H, Jørgensen BB. Microelectrode studies of seasonal oxygen uptake in a coastal
563 sediment: role of molecular diffusion. *Marine Ecology Progress Series* **81**, 289–303
564 (1992).

565 Rassmann J, Lansard B, Gazeau F, Guidi-Guilvard L, Pozzato L, Alliouane S et al. Impact of
566 ocean acidification on the biogeochemistry and meiofaunal assemblage of carbonate-
567 rich sediments: Results from core incubations (Bay of Villefranche, NW Mediterranean
568 Sea). *Marine Chemistry* **203**, 102–119 (2018).

569 Revelle R, Suess HE. Carbon dioxide exchange between atmosphere and ocean and the
570 question of an increase of atmospheric CO_2 during the past decades. *Tellus* **9**, 18–27
571 (1957)

572 Ries JB, Ghazaleh MN, Connolly B, Westfield I, Castillo KD. Impacts of seawater saturation
573 state (Ω_A = 0.4–4.6) and temperature (10, 25 °C) on the dissolution kinetics of whole-
574 shell biogenic carbonates. *Geochimica et Cosmochimica Acta* **192**, 318–337 (2016).

575 Samukawa M, Shen C, Hopkinson BM, Matsuda Y. Localization of putative carbonic
576 anhydrases in the marine diatom, Thalassiosira pseudonana. *Photosynthesis Research*
577 **121**, 235–249 (2014)

578 Santschi P, Höhener P, Benoit G, Buchholtz-ten Brink M. Chemical processes at the
579 sediment–water interface. *Marine Chemistry* **30**, 269–315 (1990).

580 Schulz KG, Riebesell U. Diurnal changes in seawater carbonate chemistry speciation at
581 increasing atmospheric carbon dioxide. *Marine Biology* **160**, 1889–1899 (2013).

582 Soetaert K, Hofmann AF, Middelburg JJ, Meysman FJR, Greenwood J. The effect of
583 biogeochemical processes on pH. *Marine Chemistry* **105**, 30–51 (2007).

584 Subhas AV, Adkins JF, Rollins NE, Naviaux J, Erez J, Berelson WM. Catalysis and chemical
585 mechanisms of calcite dissolution in seawater. *Proceedings of the National Academy of*
586 *Sciences* **114**, 8175–8180 (2017).

587 Sunda WG, Cai W-J. Eutrophication induced CO_2-acidification of subsurface coastal waters:
588 Interactive effects of temperature, salinity, and atmospheric pCO_2. *Environmental*
589 *Science and Technology* **46**, 10651–10659 (2012).

590 Tachibana M, Allen AE, Kikutani S, Endo Y, Bowler C, Matsuda Y. Localization of putative
591 carbonic anhydrase in two marine diatoms, *Phaeodactylum tricornutum* and
592 *Thalassiosira pseudonana*. *Photosynthesis Research* **109**, 205–221 (2011)

593 Ullman WJ, Aller RC. Diffusion coefficients in nearshore marine sediments. *Limnology &*
594 *Oceanography* **27**(3), 552–556 (1982).

595 Vopel K, Del-Río C, Pilditch CA. Effects of CO_2 enrichment on benthic primary production and
596 inorganic nitrogen fluxes in two coastal sediments. *Scientific Reports* **8**, 1035 (2018).

597 Vopel K, Laverock B, Cary C, Pilditch CA. Effects of warming and CO_2 enrichment on O_2
598 consumption, porewater oxygenation and pH of subtidal silt sediment. *Aquatic Sciences*
599 **83**, 8 (2021).

600 Zhu Q, Aller RC, Fan Y. Two-dimensional pH distributions and dynamics in bioturbated marine
601 sediments. *Geochimica et Cosmochimica Acta* **70**, 4933–4949 (2006).

602

Supplementary material

Biogeochemical feedbacks to ocean acidification in a cohesive photosynthetic sediment

Kay Vopel, Alexis Marshall, Shelly Brandt, Adam Hartland, Charles Lee, Craig Cary, Conrad A. Pilditch

Table S1. Sediment properties. Average (± 1 SD, n = 4) properties of the upper 10 mm layer of silt cores modified by addition of a 1-mm layer of sand (Control) or calcite (Treatment). These core were submerged in ambient or CO_2 enriched seawater.

	Ambient seawater		CO_2 enriched seawater	
	Sand	Calcite	Sand	Calcite
Silt/clay content (% volume <63 µm)	74.4 ± 4.5	80.7 ± 1.1	77.0 ± 1.0	80.3 ± 1.9
Median grain size (µm)	26.7 ± 4.4	22.5 ± 1.5	24.8 ± 1.3	22.8 ± 2.8
Water content (% dry weight)	67.2 ± 1.7	68.0 ± 0.6	66.2 ± 1.9	67.1 ± 2.1
Organic matter content (% dry weight)	8.4 ± 0.2	10.4 ± 0.0	8.6 ± 0.1	10.0 ± 0.1
$CaCO_3$ content (% dry weight)	3.8 ± 0.3	5.0 ± 0.4	3.8 ± 0.2	4.6 ± 0.2
Chl *a* (µg [g dw]$^{-1}$)	11.3 ± 1.0	14.4 ± 4.6	15.0 ± 4.1	15.1 ± 2.6
Phaeopigments (µg [g dw]$^{-1}$)	18.1 ± 1.9	21.2 ± 0.6	18.5 ± 1.8	19.4 ± 2.7
Ratio Chl *a*/phaeopigments	0.6 ± 0.1	0.7 ± 0.2	0.8 ± 0.2	0.8 ± 0.1

Table S2. Summary of two-way ANOVA *p* values testing for the effects of seawater pCO_2 (ambient, enriched) and sediment surface deposit (sand, calcite) on photosynthetic pigments.

	pCO_2	Deposit	pCO_2 × Deposit
Chl *a*	0.2137	0.3608	0.3916
Phaeopigments	0.5154	0.0571	0.2873
Chl *a*/phaeopigments	0.0676	0.8662	0.6192

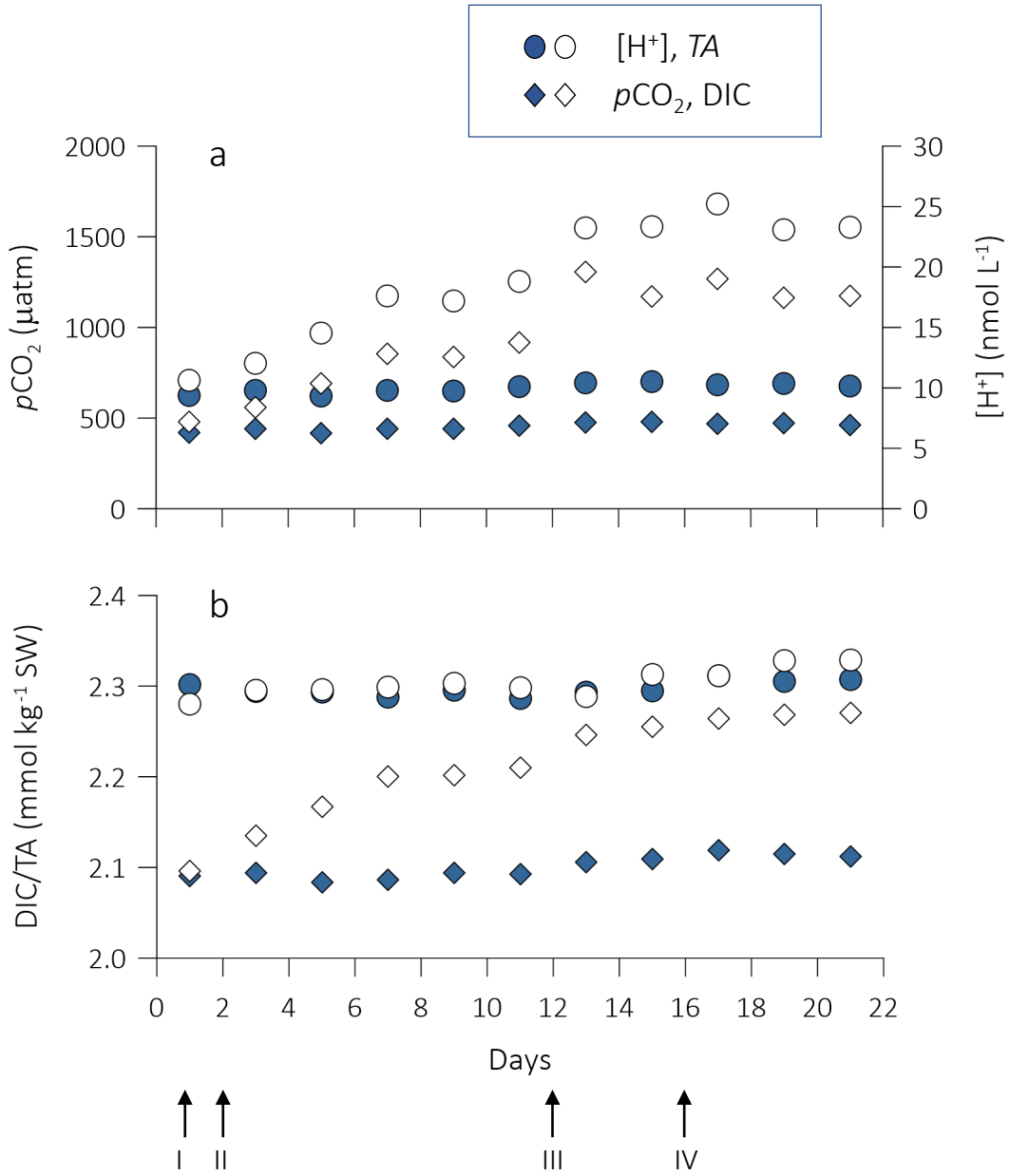

619

620 **Figure S1** Experimental time line (I-IV) and time series of (**a**) seawater pCO_2, $[H^+]$ and (**b**) dissolved
621 inorganic carbon concentration (DIC), and total alkalinity (TA) in two seawater recirculating
622 experimental units. The seawater in one unit (open symbols) was gradually enriched with CO_2.
623 Diamonds, DIC and pCO_2. Circles, TA and $[H^+]$. Arrows: I, application of sand (Control) and calcite
624 (Treatment) deposits; II, injection of CO_2 started to stepwise increase the seawater pCO_2; III, CO_2
625 injection maintains pCO_2 at 1216 ± 88 µatm; IV, microprofiling measurements start. See text for
626 further details.

627

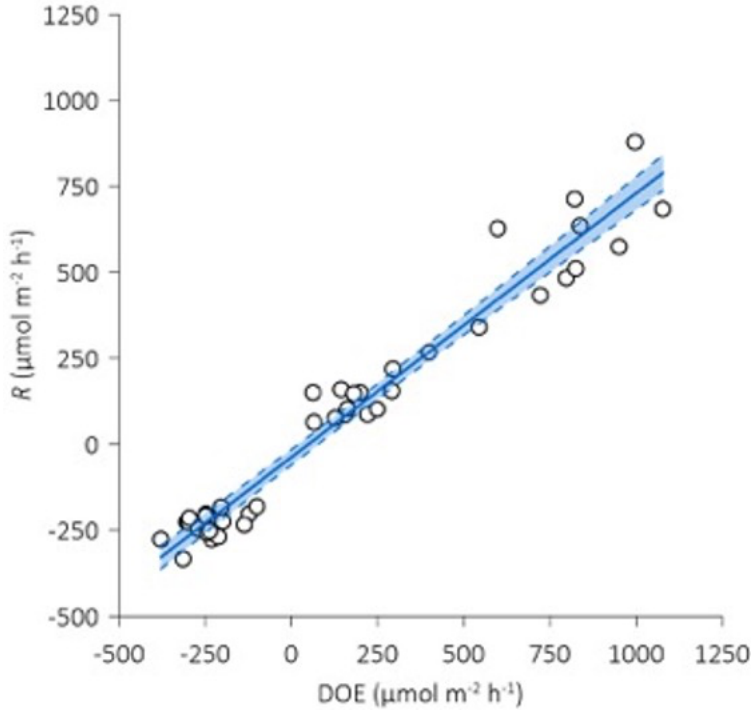

628

629 **Figure S2** Scatter plot showing the linear relationship between the diffusive O_2 exchange (DOE) across
630 the diffusive boundary layer (DBL), and the areal depth-integrated O_2 consumption, R_A. The former
631 was derived from [O_2] microprofiles in the DBL, whereas the latter was from porewater [O_2]
632 microprofiles. The solid and dashed lines indicate respectively the linear fit (R^2 = 0.96) and 95%
633 confidence intervals.